



Pt–Fe catalyst nanoparticles supported on single-wall carbon nanotubes: Direct synthesis and electrochemical performance for methanol oxidation



Xiaohui Ma ^a, Liqiang Luo ^b, Limei Zhu ^b, Liming Yu ^a, Leimei Sheng ^a, Kang An ^a, Yoshinori Ando ^c, Xinluo Zhao ^{a,*}

^a Department of Physics and Institute of Low-dimensional Carbons and Device Physics, Shanghai University, Shanghai 200444, PR China

^b Departments of Chemistry, Shanghai University, Shanghai 200444, PR China

^c Departments of Materials Science and Engineering, Meijo University, Nagoya 468-8502, Japan

HIGHLIGHTS

- One-step preparation of Pt–Fe catalyst nanoparticles supported on SWCNTs.
- The catalyst performs high electrocatalytic activity and better stability.
- Avoid additional treatment to protect the crystallinity of SWCNTs.
- Their high electronic conductivity lowers resistance in methanol electrooxidation.

ARTICLE INFO

Article history:

Received 27 December 2012

Received in revised form

20 April 2013

Accepted 22 April 2013

Available online 29 April 2013

Keywords:

Carbon nanotubes

Catalyst

Methanol oxidation

Fuel cells

Platinum

ABSTRACT

Single-wall carbon nanotubes (SWCNTs) supported Pt–Fe nanoparticles have been prepared by one-step hydrogen arc discharge evaporation of carbon electrode containing both Pt and Fe metal elements. The formation of SWCNTs and Pt–Fe nanoparticles occur simultaneously during the evaporation process. High-temperature hydrogen treatment and hydrochloric acid soaking have been carried out to purify and activate those materials in order to obtain a new type of Pt–Fe/SWCNTs catalyst for methanol oxidation. The Pt–Fe/SWCNTs catalyst performs much higher electrocatalytic activity for methanol oxidation, better stability and better durability than a commercial Pt/C catalyst according to the electrochemical measurements, indicating that it has a great potential for applications in direct methanol fuel cells.

© 2013 Elsevier B.V. All rights reserved.

1. Introduction

Direct methanol fuel cells (DMFCs) are attractive alternatives to combustion engines in transportation applications for electrical power generation and also regarded as promising future power sources, especially for mobile and portable applications due to their high energy density properties. Platinum-based nanoparticles supported on carbon-black (e.g., Pt/C) are commonly employed as an electrocatalyst in DMFCs [1]. However, carbon support corrosion and platinum nanoparticles dissolution/aggregation in the operating environment usually result in the activity loss and the

durability shortening of catalyst. An efficient way to achieve better activity and durability of Pt-based catalyst nanoparticles is to disperse them onto a suitable support, which should fulfill the following requirements: the support needs to have (1) a high surface area and strong affinity for the catalyst nanoparticles to ensure their efficient immobilization in a well-dispersed way, (2) a high electrical conductivity to facilitate fast electron transfer in many redox reactions, (3) an excellent chemical stability in the operating environment to maintain a stable catalyst structure [2].

Compared to the conventional carbon-black support, carbon nanotubes (CNTs) have been demonstrated as a kind of advanced support material for Pt and Pt-based nanoparticles [3–10]. Nevertheless, for better catalyst nanoparticle immobilization, the CNTs usually require a suitable surface functionalization pretreatment, such as acid oxidation [11,12], ionic liquid linking [13–15], polymer

* Corresponding author. Tel.: +86 21 66136916; fax: +86 21 66134208.

E-mail address: xlzhao@shu.edu.cn (X. Zhao).

wrapping [16–18], plasma treatment [19], and so on. These functionalization pretreatments might cause a partial destruction of the CNT structure that leads to a decrease in its electrical conductivity [20]. In particular, single-wall carbon nanotubes (SWCNTs) possess smaller size, fewer defects, much better conductivity, higher surface area and larger surface-to-volume ratio compared with the multiwalled nanotubes (MWCNTs). Therefore, SWCNTs should be more suitable as a catalyst support, but very few reports could be found in the literature to prove such an important issue [21–24].

In our previous study, we have developed a technique for mass production of high-crystallinity SWCNTs with embedded Fe nanoparticles, by using hydrogen arc discharge evaporation of carbon electrode containing Fe catalyst [25]. The Fe nanoparticles have been found to be wrapped with several layers of graphene sheets, which can be eliminated by a simple purification process, for example, heating in hydrogen atmosphere at 1073 K, and washing with hydrochloric acid [26]. Sergienko et al. have reported that PtFe nanoparticles included in few layer graphene sheets can be synthesized by an arc evaporation of PtFe electrode in an ultrasonic cavitation field of liquid ethanol [27]. A disordered face-centered cubic (fcc) structure (γ Fe, Pt) was revealed by using transmission electron microscopy (TEM) and X-ray diffraction (XRD).

Here, we report the direct synthesis of Pt–Fe catalyst nanoparticles supported on SWCNTs by hydrogen arc discharge evaporation of carbon electrode containing both Pt and Fe catalysts. A high-temperature hydrogen treatment has been used to remove the graphene sheets that are encapsulating Pt–Fe catalyst nanoparticles. The electrocatalytic activity of this Pt–Fe/SWCNTs catalyst was then studied by cyclic voltammetry and chronoamperometry, showing excellent catalytic performance and better durability for methanol oxidation.

2. Experimental

2.1. Catalyst preparation

The SWCNTs supported Pt–Fe nanoparticles were prepared by using an apparatus of dc arc discharge evaporation similar as our former studies [25]. Two electrodes were installed vertically at the center of a water-cooled stainless steel chamber. The upper cathode was a pure carbon rod (10 mm in diameter, 30 mm long), and the bimetallic catalyst doped carbon anodes were prepared as follows: carbon rods doped homogeneously with 1 at.% Fe catalyst (6 mm in diameter, 30 mm long) were hollowed out (20 mm in depth, 4.2 mm in diameter) and filled with a mixture of graphite powder and Pt catalyst powder. The atomic ratio of Fe to Pt in doped carbon anodes was 1:1. A dc arc discharge was generated by applying 60 A in H_2 –Ar or H_2 –He atmosphere (2:3/v:v) at a total pressure of 200 torr. During arc discharge, the distance between two electrodes was kept constantly about 2 mm. After arc evaporation for \sim 2 min, some web-like products were collected from the inner wall of the chamber (marked as as-grown SWCNTs).

For synthesizing Pt–Fe/SWCNTs catalyst for methanol oxidation, the as-grown SWCNTs were heated at 1073 K in H_2 –Ar mixture gas (1:4/v:v) with a total flow rate of 100 sccm for 1 h to remove the graphene sheets that are encapsulating Pt–Fe catalyst nanoparticles (marked as H_2 -treated SWCNTs). In order to dissolve redundant Fe metal and its oxide nanoparticles, these H_2 -treated SWCNTs were soaked in concentrated hydrochloric acid. After this procedure, the samples were designated as Pt–Fe/SWCNTs, and used in the following electrochemical measurements.

2.2. Catalyst characterization

The as-grown SWCNTs, H_2 -treated SWCNTs and Pt–Fe/SWCNTs samples were characterized by scanning electron microscopy (SEM,

JEOL JSM-6700F) equipped with an energy-dispersive X-ray analysis system (EDS, OXFORD INCA EDS), TEM (JEOL JEM-200CX) and high-resolution TEM (HRTEM, JEOL JEM-2010F). Raman spectra were recorded using a Raman spectrometer (Renishaw InVia-plus) with 785 nm excitation.

2.3. Electrochemical measurement

Electrochemical measurements were carried out by a CHI660C electrochemical workstation (Chenhua Co. Ltd. Shanghai, China) in a conventional three-electrode cell. A glassy carbon electrode (GCE, $\Phi = 3$ mm) modified by catalysts was used as a working electrode, a saturated calomel electrode (SCE) for the reference electrode, and a platinum sheet for the counter electrode. The Pt–Fe/SWCNTs catalyst layer on GCE was prepared as follows: about 1 mg Pt–Fe/SWCNTs catalyst was added to a mixture solution containing 200 μ L alcohol (95%) and 20 μ L Nafion (5 wt%), and then ultrasonicated for over 1 h to obtain a homogeneous black ink solution. Afterwards 21 μ L of the black ink was spread on a clean GCE surface. The electrode was dried at 90 °C for 1 h in air to obtain a thin and even catalytic layer.

For cyclic voltammetry and chronoamperometry (CA) of methanol oxidation, the electrolyte solution was 1 M CH_3OH in 0.5 M H_2SO_4 . All experiments were performed at room temperature, and the sweep rate is 50 mV s⁻¹. High-purity N_2 was bubbled into the electrolyte during the whole electrochemical experiment.

Electrocatalyst durability was evaluated by cycling the electrode potential between 0 and 1.0 V versus SCE at a scan rate of 50 mV s⁻¹ in 1 M CH_3OH and 0.5 M H_2SO_4 solution at room temperature. Because the concentration of methanol falls down during the test, and it is hard to evaluate the real activity for methanol oxidation, we chose the electrochemical surface area (ECSA) as the sign of activity. After each 100 cycles, three additional cycles in 0.5 M H_2SO_4 solution between –0.25 and 1.0 V versus SCEs were used to calculate their ECSA. Those ECSAs were normalized to the initial values, and plotted as a function of cycle numbers. The commercial Pt/C catalyst (JM HiSPEC 4000, 38.04 wt%) was also employed for the same test for comparison. After durability test, the solution was renewed and an additional 100 cycles were recorded to evaluate the loss of catalyst activity.

3. Results and discussion

Fig. 1a shows a typical SEM image of as-grown SWCNTs sample. The bright spots on the surface of SWCNT bundles are from metal catalyst nanoparticles. TEM observations, as shown in Fig. 1b, indicated that the long bundles of SWCNTs have diameters of 10–40 nm, and Pt–Fe catalyst nanoparticles are nearly spherical and uniformly dispersed on the external surface of SWCNTs. In this low-magnification TEM image, these metal nanoparticles are observed as dark dots with a size range from 2 to 20 nm.

A selected-area electron diffraction (SAED) pattern of TEM image is presented in the inset of Fig. 1b. The innermost reflection ring, marked as G (002), is associated with the (002) diffraction of the hexagonal graphite structure in as-grown SWCNTs samples, and has been used for calibration. Three reflection rings, (111), (200), and (220), indicate the abundant existence of face-centered cubic (fcc) structure, in which Fe and Pt atoms are randomly packed. There are some diffraction spots from the body-centered cubic (bcc) structure of α -Fe phase, such as (110) and (200), suggesting the existence of pure Fe nanoparticles. The extra reflection rings such as (001) and (110) which indicate the chemically ordered face-centered tetragonal (fct) phase, are hardly observed between G (002) ring and (111) reflection ring of fcc structure (γ Fe, Pt). The XRD profile has been also measured, and it is consistent with the results of SAED patterns. HRTEM observations indicate that the

Pt–Fe metal nanoparticles are embedded within graphene sheets, which substantially hampers their electrocatalytic activity.

In order to remove the graphene sheets which are encapsulating Pt–Fe metal nanoparticles, the as-grown SWCNTs samples were annealed at 1073 K in an atmosphere of H₂–Ar mixture gas (1:4/v:v) for 1 h. A typical low-magnification TEM image of H₂-treated SWCNTs samples is shown in Fig. 2a. It is interesting to note that the metal nanoparticles become bigger after annealing, and their shapes have changed from spheroid to cube due to fusion between them. The inset of Fig. 2a is an HRTEM image of the metal nanoparticles. It has been confirmed that most of the graphene sheets enwrapping Pt–Fe metal nanoparticles have been removed, and there are some metal nanoparticles lying on the half opened carbon shells, which look like carbon bowls. It can be expected that

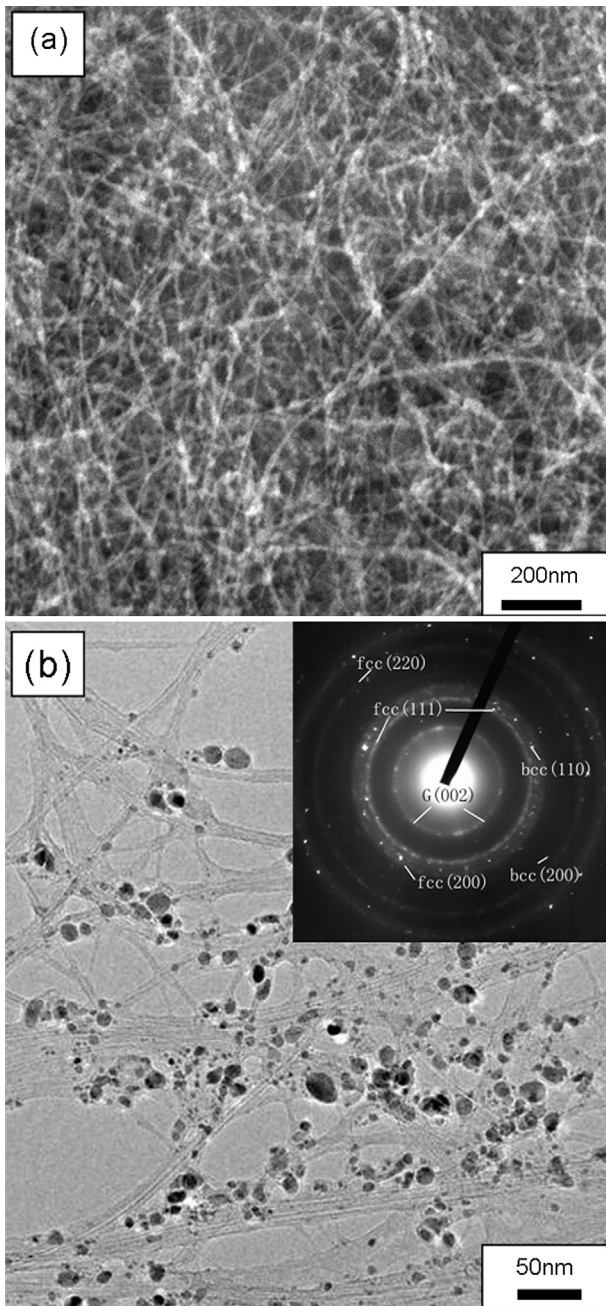


Fig. 1. (a) SEM image of as-grown SWCNTs; (b) TEM image of as-grown SWCNTs, and the inset shows its SAED pattern.

these carbon shells attaching on the surface of SWCNTs will act as the anchor points, preventing the aggregation of Pt–Fe metal nanoparticles in the operating environment in DMFCs.

Fig. 2b shows the histogram of Pt–Fe nanoparticle size, which has been obtained by measuring the sizes of 300 randomly chosen nanoparticles in magnified TEM images. It is found that the Pt–Fe nanoparticles have a size distribution of 2–20 nm, and the average size is 7.1 nm in the case of as-grown SWCNTs. After high-temperature hydrogen treatment, the average size of Pt–Fe nanoparticles changes to 8.2 nm, and several nanoparticles are even larger than 40 nm (not shown). The average size of Pt–Fe nanoparticles in Pt–Fe/SWCNTs samples is ranged in between 7.1 and 8.2 nm.

Fig. 3a shows the EDS spectra taken from H₂-treated SWCNTs sample, and the inset lists the EDS analysis results of as-grown SWCNTs, H₂-treated SWCNTs, and Pt–Fe/SWCNTs samples. It can be seen that the typical Pt loading in the as-grown SWCNTs sample is 18.03 wt%, and the percentage of Pt increases to 22.95 wt% after high-temperature hydrogen treatment. The decrease of carbon content in H₂-treated SWCNTs sample may be due to the burning effect of carbons which include three parts: (1) the unsaturated SWCNTs, (2) graphene sheets that are encapsulating Pt–Fe metal nanoparticles, and (3) the amorphous carbon that is coexisting with

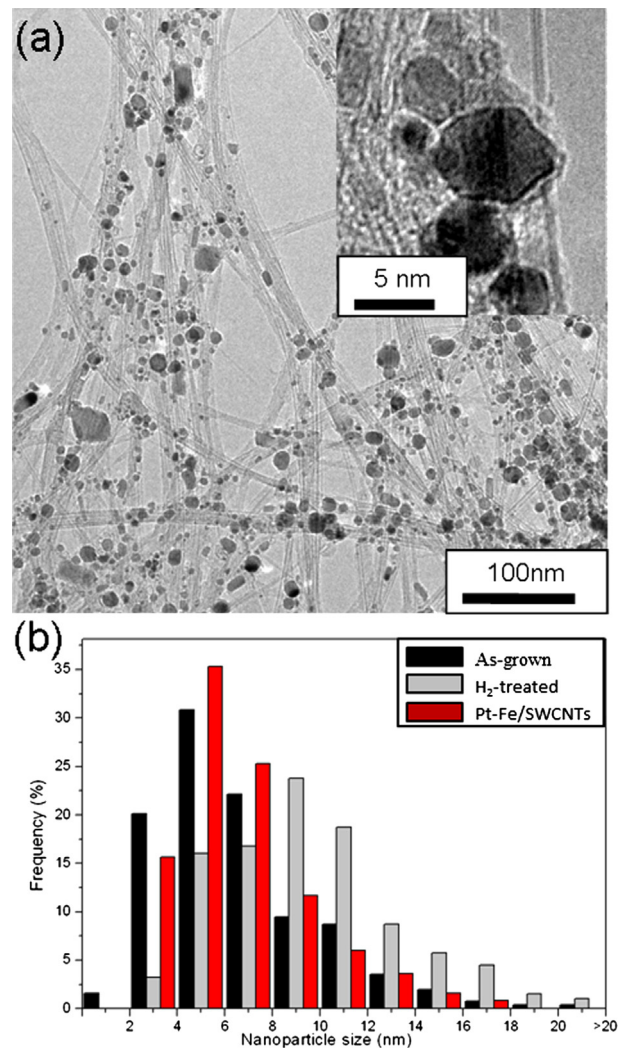


Fig. 2. (a) TEM image of H₂-treated SWCNTs, the inset is HRTEM image of metal nanoparticles; (b) histogram of Pt–Fe nanoparticle size distribution.

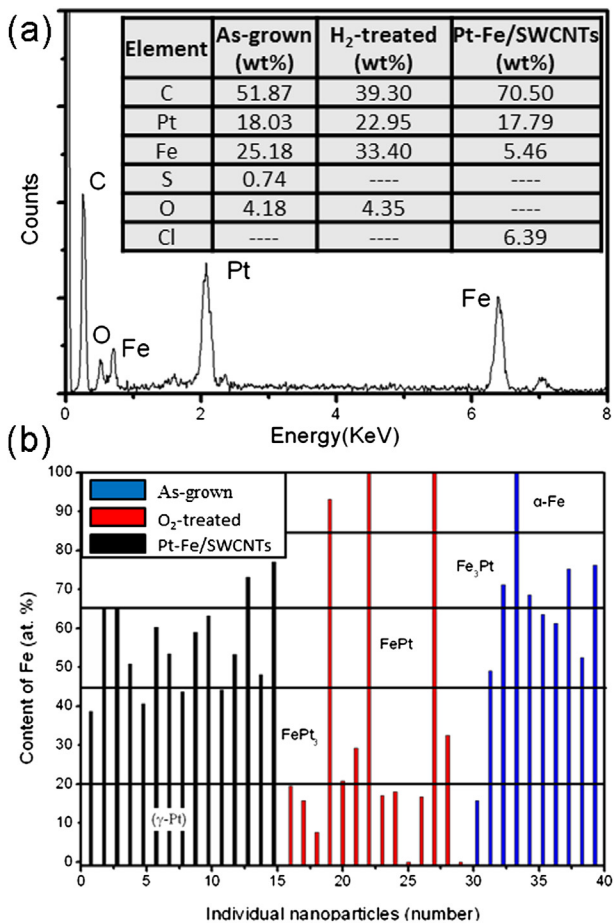


Fig. 3. (a) EDS spectra of H₂-treated SWCNTs, and the inset shows EDS analysis results of as-grown SWCNTs, H₂-treated SWCNTs and Pt-Fe/SWCNTs; (b) chemical compositions of individual Pt-Fe nanoparticles.

SWCNTs. After HCl soaking (see the EDS analysis result of Pt-Fe/SWCNTs samples), the percentage of Fe significantly decreases from 33.4 to 5.76 wt%, that of Pt slightly decreases to 17.79 wt%, that of C increases from 39.3 to 70.05 wt%, and the remaining impurity is Cl (6.39 wt%).

The chemical compositions of individual Pt-Fe nanoparticles have been also measured by EDS (OXFORD INCA EDS) equipped with HRTEM. The Fe/Pt atomic ratios were calculated from the EDS data of over ten randomly chosen nanoparticles in the HRTEM image. It has been found that the ratio is different among different samples. For the as-grown SWCNTs samples, the chemical composition is toward overstoichiometric Fe content, and the composition distribution is narrow. In the case of Pt-Fe/SWCNTs, the Fe/Pt atomic ratio is about 1:1. For comparison, we have also heated the as-grown SWCNTs samples in air at 673 K for 0.5 h, soaked the residual material in HCl, and measured the chemical compositions of individual Pt-Fe nanoparticles. Their chemical compositions, marked as O₂-treated in Fig. 3b, are very heterogeneous: some of them are saturated with Fe while the others are saturated with Pt. Therefore, it is more advantageous to use H₂ gas than air to remove the graphene sheets and unwrap the Pt-Fe catalyst nanoparticles for preparing the Pt-Fe/SWCNTs catalyst of electrochemical measurements.

Raman spectroscopy is a powerful tool for characterizing carbon nanomaterials. In the case of SWCNTs, there are three important Raman features [28]: (1) radial breathing modes (RBMs) between 100 and 300 cm⁻¹, which can be used to calculate the nanotube

diameter (d_t , nm) through the relation $\omega_{RBM} = 234/d_t + 10$; (2) G-band around 1590 cm⁻¹, which is related to the graphite in-plane vibration with an E_{2g} symmetry intralayer mode; (3) D-band (D means disorder) around 1300 cm⁻¹, which is related to the defects on SWCNTs surface and the presence of amorphous carbon in the samples. The intensity ratio of G-band to D-band (I_G/I_D) can comprehensively reflect the purity, crystallinity and structural integrity of SWCNTs.

Fig. 4 shows the Raman spectra corresponding to as-grown SWCNTs, H₂-treated SWCNTs, Pt-Fe/SWCNTs, as-grown SWCNTs prepared by using Fe catalyst only (pure Fe), and as-grown SWCNTs prepared by using Pt-Fe catalysts in H₂-He atmosphere (as-grown in H₂-He). For ease of comparison, the Raman spectra have been normalized to the intensity of G-band. Using the relation mentioned above, the RBM peaks at 150, 200, 229 and 264 cm⁻¹ can be assigned to the SWCNTs with the diameters of 1.67, 1.23, 1.09 and 0.92 nm, respectively. The spectrum of as-grown SWCNTs prepared in H₂-He atmosphere is very similar to that of the as-grown SWCNTs prepared by using Fe catalyst only. It can be seen that the addition of Pt catalyst results in the intensity increase of the RBM at 150 cm⁻¹. This means the abundant existence of thick SWCNTs with the diameter of 1.67 nm in the samples. Compared with the as-grown SWCNTs prepared by using Fe catalyst only, the D-band intensity of the as-grown SWCNTs is stronger. Obviously, the presence of Pt atom in arc plasma hampers the catalytic activities of Fe atom in the formation of SWCNTs. Using H₂-He atmosphere to replace H₂-Ar atmosphere can change the diameter distribution of SWCNTs, and make the thin SWCNTs with the diameters of 1.09 nm become relatively plentiful. The high-temperature hydrogen treatment leads to the disappearance of

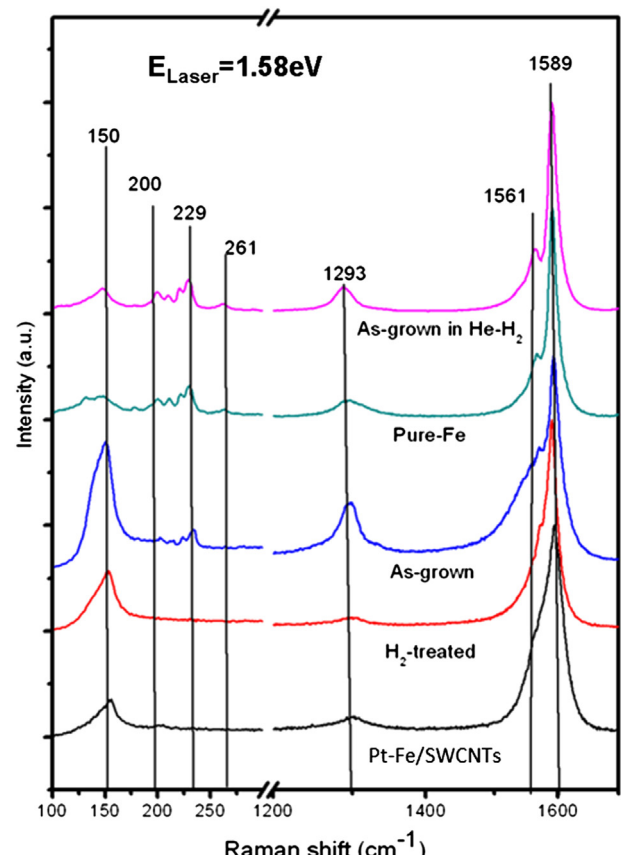


Fig. 4. Raman spectra taken from five different SWCNTs samples.

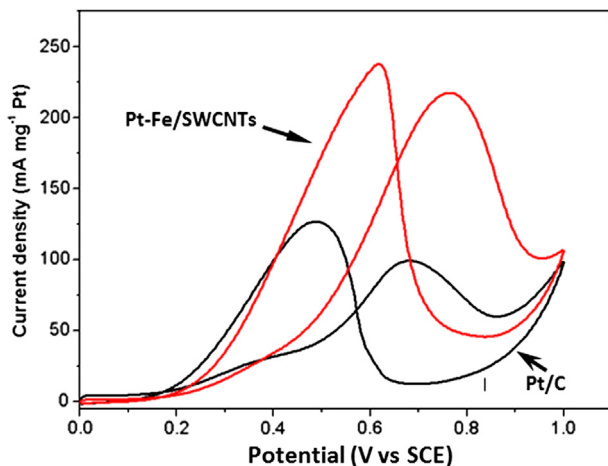


Fig. 5. Cyclic voltammograms of commercial Pt/C catalyst (JM HiSPEC 4000) and Pt-Fe/SWCNTs catalyst, measured in 1 M CH_3OH + 0.5 M H_2SO_4 aqueous solution, saturated with N_2 . The sweep rate is 50 mV s^{-1} .

D-band, and increases the intensity ratio of I_G/I_D , indicating the dramatic decrease of amorphous carbon in SWCNTs samples.

Fig. 5 exhibits the typical cyclic voltammograms (CVs) of the Pt-Fe/SWCNTs catalyst (Pt 17.7%) with Pt loading of $520 \mu\text{g cm}^{-2}$ and the commercial Pt/C catalyst (JM HiSPEC 4000) with Pt loading of $543 \mu\text{g cm}^{-2}$. They were measured at the sweep rate of 50 mV s^{-1} in the potential range between 0.0 and 1.0 V in 1 M CH_3OH and 0.5 M H_2SO_4 aqueous solution. After several cycles, the cyclic voltammetry became stable. The voltammetric features are in good agreement with literature [29], in which the typical methanol oxidation current peak on Pt catalyst is at about 0.84 V vs SCE in the forward scan, and an oxidation current peak is at about 0.59 V vs SCE in the backward scan, related to the oxidation of the corresponding intermediates produced during methanol oxidation. For easy to comparison, we used similar catalyst loading, and the plot was normalized with the platinum mass. While the as-grown SWCNTs or the purified SWCNTs samples were used as electrode, there was no current response for methanol oxidation, indicating that SWCNTs are not active for methanol oxidation and the graphene sheets enwrapping Pt-Fe metal nanoparticles must be removed. In the case of H_2 -treated SWCNTs samples, it shows similar CV characteristics as the Pt-Fe/SWCNTs samples, except an obvious reduction peak at reverse scan in the initial few cycles, indicating that there is redundant Fe and the HCl soaking is necessary. It is worth mentioning that the forward peak current density of Pt-Fe/SWCNTs is about 1.5 times higher than that of the commercial 40% Pt/C catalyst.

To further assess steady state catalyst performance with respect to methanol electrooxidation, we have carried out CA tests at a series of steady potentials. Fig. 6 presents the examples of the CA curves obtained in 1 M CH_3OH + 0.5 M H_2SO_4 at different polarization potential. The CA curve of the commercial 40% Pt/C catalyst is also recorded at the potential of 0.63 V. For the ease of comparison, the Pt loading of all tests was $520 \mu\text{g cm}^{-2}$. It can be found that in

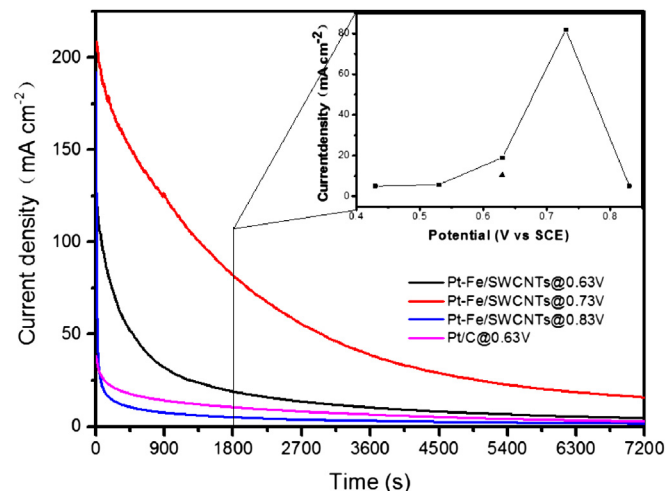


Fig. 6. Chronoamperometry of commercial Pt/C catalyst (JM HiSPEC 4000) and Pt-Fe/SWCNTs catalyst at different polarized potential, measured in 1 M CH_3OH + 0.5 M H_2SO_4 aqueous solution, saturated with N_2 . The inset is the current density recorded at 1800 s at different polarized potential.

the all CA curves the potentiostatic current density decreases rapidly in the initial time period, achieves a pseudosteady state after a period of 900 s, and then decays slightly with time. The rapidly decreases of current density could be due to the formation of intermediate species during the methanol oxidation reaction. In general, if the kinetics of the removal for intermediate species is poor, the decreases of the current density will be fast, a gradual decay of current density with time implies that the catalyst has good anti-poisoning ability. After 30 min of polarization at 0.63 V (at 25 °C), the Pt-Fe/SWCNTs electrode had a current density of approximately 19 mA cm^{-2} , compared with the current densities of approximately 11 mA cm^{-2} for the commercial 40% Pt/C electrode. Moreover, the current decayed more slowly for the Pt-Fe/SWCNTs than the commercial catalysts, indicating less accumulation of adsorbed CO species. All those results imply that the Pt-Fe/SWCNTs catalyst exhibits higher catalytic activity and better stability than the commercial catalysts.

Furthermore, the current densities are also dependent on the use of polarization voltage. The current densities recorded after 30 min of polarization are shown in the inset of Fig. 6. It can be found that the current densities are increased with the polarized potential. But when the polarized potential is up to 0.83 V, the current densities decrease very fast. These results indicate that the Pt-Fe/SWCNTs electrode polarized with 0.83 V deactivates at a faster rate. We therefore conclude that the Pt-Fe/SWCNTs electrode polarized at 0.73 V has better electrocatalytic activity for methanol oxidation.

There are two ways to estimate the activities of Pt-based electrocatalysts. One is mass activity (MA) associated with the current per amount of catalyst, and the other is specific activity (SA) related to the surface area of Pt. The MA has significant implications for fuel cells, because the cost of electrode largely depends on the total

Table 1
Summary of various electrochemical parameters.

	Initial ECSA ($\text{m}^2 \text{ g}^{-1}$)	ECSA after 1000 cycles ($\text{m}^2 \text{ g}^{-1}$)	ECSA loss (%)	Forward peak current density, i_f (mA cm^{-2})	Forward peak current potential (V)	i_f/i_b ratio	Mass activity ($\text{mA mg}^{-1} \text{ Pt}$)	Specific activity ($\text{mA cm}^{-2} \text{ Pt}$)	i_f after 1000 cycles (mA cm^{-2})	i_f loss (%)
Pt-Fe/SWCNTs	86.37	44.52	48.46	194.12	0.81	0.97	373.11	4.31	112.33	42.29
Pt/C	204.08	51.62	74.71	147.2	0.73	0.74	270.71	1.32	41.11	72.11

catalysts, while the SA provides the catalytic information of Pt atoms in the surface of catalyst. The various parameters, including MA (peak current density of methanol oxidation obtained from CV per unit of Pt loading mass), SA (peak current normalized with Pt surface area), and the ratio of the forward oxidation current peak (i_f) to the reverse current peak (i_b), have been shown in Table 1. According to the MA data listed in Table 1, the Pt–Fe/SWCNTs catalyst shows better electrocatalytic activities for methanol oxidation than the commercial Pt/C catalyst. It can be also seen that the SA of Pt–Fe/SWCNTs catalyst is extremely higher (about 3.3 times) than commercial ones. The i_f/i_b ratio is an index of the catalyst tolerance to CO species. From Table 1, the i_f/i_b ratio of Pt–Fe/SWCNTs catalyst is slightly higher than that of the commercial Pt/C catalyst, indicating that the new Pt–Fe/SWCNTs catalyst can more effectively remove the CO species on their surface.

The ECSA is a useful macroscopic quantity to characterize the dispersed catalysts. For Pt-based catalysts, it can be calculated from the hydrogen desorption peaks formed in the lower potential region of CV curve in H_2SO_4 solutions. In the calculated data in Table 1, it can be found that the ECSA value of our samples is one fourth of the commercial ones. This may be attributed to the big particle size of our samples, resulting in that the total surface area of our samples is less than the commercial ones.

Long-term structural durability is one of the characteristics most necessary for fuel cells to be accepted as a viable product. Thus, in addition to the electrocatalytic activity, the durability of Pt–Fe/SWCNTs has also been evaluated by repetitive potential cycling test. The ECSA loss and electrocatalytic activity decrease were used as indicator for the durability. Fig. 7 shows the electrocatalyst durability of commercial Pt/C catalyst and Pt–Fe/SWCNTs catalyst. It can be seen that the ECSA of Pt–Fe/SWCNTs catalyst decrease slower than the commercial Pt/C catalyst. After 1000 cycles, the solution was renewed and an additional 100 cycles in 1 M CH_3OH and 0.5 M H_2SO_4 solution were recorded so as to evaluate the loss of catalyst activity. The various electrochemical parameters have been summarized in Table 1. It can be seen that the Pt–Fe/SWCNTs catalyst remains 51.54% ECSA and 57.71% activity after 1000 cycles, while the data for commercial Pt/C catalyst are 25.29% and 27.89%, indicating that the new type Pt–Fe/SWCNTs catalyst is more durable than commercial ones.

Fig. 8 illustrates the morphological and chemical changes of Pt–Fe nanoparticle on SWCNTs surface during the synthesis process of Pt–Fe/SWCNTs catalyst. In the as-grown SWCNTs samples, the Pt–Fe metal nanoparticles are anchored on the side wall of SWCNTs, and enwrapped by graphene sheets which hamper the

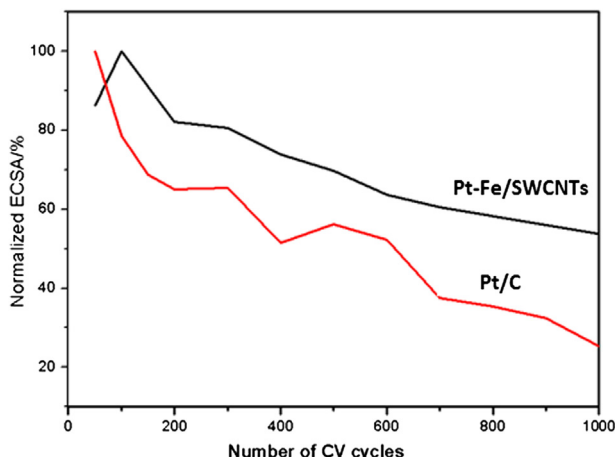


Fig. 7. Electrocatalyst durability of commercial Pt/C catalyst (JM HiSPEC 4000) and Pt–Fe/SWCNTs catalyst.

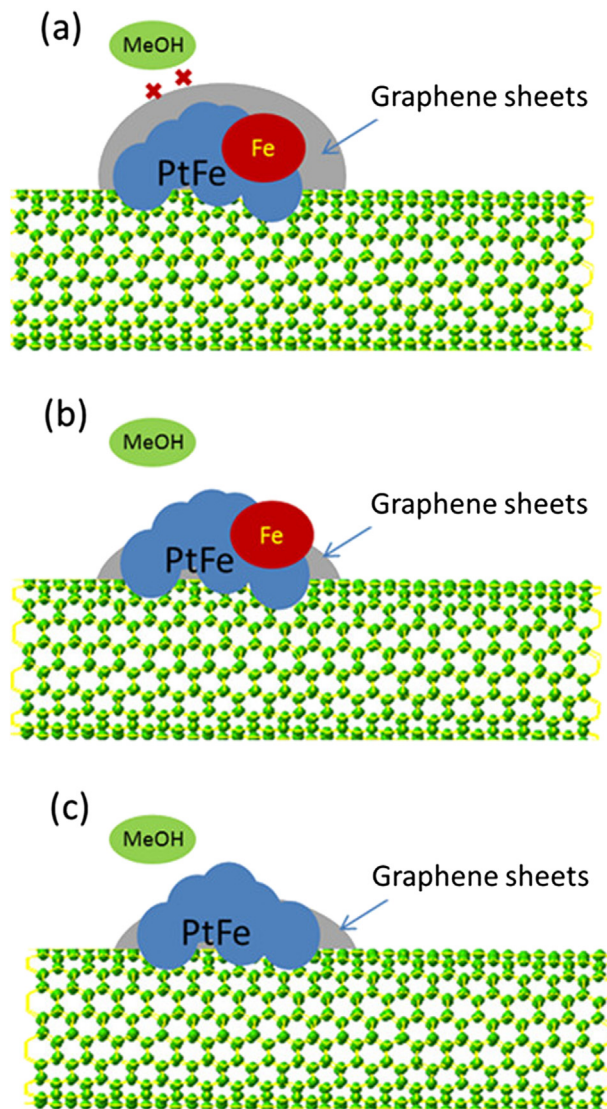


Fig. 8. Illustration of morphological and chemical changes of Pt–Fe nanoparticle on the surface of (a) as-grown SWCNT, (b) H_2 -treated SWCNT, and (c) SWCNT after HCl soaking.

electrocatalytic activity of Pt-based catalyst. After a high-temperature hydrogen treatment, the graphene shells have been exfoliated. After HCl soaking, the metal nanoparticles shrink, and the chemical composition of metal nanoparticles transforms toward overstoichiometric Pt content.

Conventionally, the electrocatalyst with high percentage composition (e.g., total Pt catalyst percentage > 60 wt%) are desirable for DMFC applications. The present Pt–Fe/SWCNTs catalyst has a much lower composition percentage of about 20 wt% based on the EDS analysis results, but it performs much higher catalytic activity and better stability. The high catalytic activity and good stability can be attributed to several factors: (i) the Pt–Fe/SWCNTs electrocatalyst possesses perfect nanoparticle sizes and ideal compositions that enhance its electrocatalytic activity, (ii) the high electronic conductivity of high-crystallinity SWCNTs lowers the resistance in methanol electrooxidation, (iii) the half carbon shells attaching on the surface of SWCNTs prevent the aggregation of the uniformly dispersed Pt–Fe electrocatalyst nanoparticle, (iv) the synergistic effect resulting from the coexistence of graphene carbon, Pt and Fe. It should be pointed out that the as-grown SWCNTs samples and H_2 -treated SWCNTs samples have not

performed good electrocatalytic activity as the Pt–Fe/SWCNTs samples, showing the necessity of removing both the carbon shells from Pt–Fe electrocatalyst nanoparticle and the residual Fe catalyst in H₂-treated SWCNTs samples. Furthermore, it must be mentioned that the composition of the nanoparticles in bimetallic systems is also make good effect with the electrocatalytic activity [30], and a systemic research of different synthesis conditions for compositional studies has been planned in the further works.

4. Conclusions

Pt–Fe catalyst nanoparticles supported on SWCNTs can be prepared in one-step by hydrogen arc discharge evaporation of carbon electrode containing Pt and Fe catalyst. A simple high-temperature hydrogen treatment of as-grown SWCNTs can remove the graphene sheets which are encapsulating Pt–Fe catalyst nanoparticles. After soaking the H₂-treated SWCNTs in concentrated hydrochloric acid, a new type of Pt–Fe/SWCNTs electrocatalyst, which performs much higher electrocatalytic activity for methanol oxidation, better stability and better durability than a commercial Pt/C catalyst, has been successfully obtained. The detailed electrochemical measurement results indicate that this novel Pt–Fe/SWCNTs electrocatalyst has great potential in the application of direct methanol fuel cells.

Acknowledgments

This work is supported by the National Natural Science Foundation of China (Grant Nos. 10974131, 51202137, 61240054 and 11274222). Acknowledgments are also made to the Instrumental Analysis and Research Center of Shanghai University. Special thanks are due to Prof. W. Ren of Shanghai University for valuable comments.

References

- [1] H.S. Liu, C.J. Song, L. Zhang, J.J. Zhang, H.J. Wang, D.P. Wilkinson, *J. Power Sources* 155 (2006) 95–110.
- [2] E. Antolini, *Appl. Catal. B* 88 (2009) 1–24.
- [3] B. Qu, Y.T. Xu, S.J. Lin, Y.F. Zheng, L.Z. Dai, *Synth. Met.* 160 (2010) 732–742.
- [4] W. Li, C. Liang, W. Zhou, J. Qiu, Z. Zhou, G. Sun, Q. Xin, *J. Phys. Chem. B* 107 (2003) 6292–6299.
- [5] A.S. Afolabi, A.S. Abdulkareem, S.E. Iyuke, H.C.V.Z. Pienaar, *J. Mater. Res.* 27 (2012) 1497–1505.
- [6] A. Abedini, B. Dabir, M. Kalbasi, *Int. J. Hydrogen Energy* 37 (2012) 8439–8450.
- [7] S.S.J. Aravind, S. Ramaprabhu, *ACS Appl. Mater. Interfaces* 4 (2012) 3805–3810.
- [8] C. Wang, B. Li, H. Lin, Y. Yuan, *J. Power Sources* 202 (2012) 200–208.
- [9] J. Qian, W. Wei, X. Huang, Y. Tao, K. Chen, X. Tang, *J. Power Sources* 210 (2012) 345–349.
- [10] D.-J. Guo, J.-M. You, *J. Power Sources* 198 (2012) 127–131.
- [11] A. Halder, S. Sharma, M.S. Hegde, N. Ravishankar, *J. Phys. Chem. C* 113 (2009) 1466–1473.
- [12] Z. Cui, C. Liu, J. Liao, W. Xing, *Electrochim. Acta* 53 (2008) 7807–7811.
- [13] S.J. Guo, S.J. Dong, E.K. Wang, *Adv. Mater.* 22 (2010) 1269–1271.
- [14] B. Wu, D. Hu, Y. Kuang, B. Liu, X. Zhang, J. Chen, *Angew. Chem. Int. Ed.* 48 (2009) 4751–4754.
- [15] B. Wu, D. Hu, Y. Yu, Y. Kuang, X. Zhang, J. Chen, *Chem. Commun.* 46 (2010) 7954–7956.
- [16] M. Okamoto, T. Fujigaya, N. Nakashima, *Small* 5 (2009) 735–740.
- [17] B. Ritz, H. Heller, A. Myalitsin, A. Kornowski, F.J. Martin-Martinez, S. Melchor, J.A. Dobado, B.H. Juarez, H. Weller, C. Klinke, *ACS Nano* 4 (2010) 2438–2444.
- [18] S. Li, X. Yu, G. Zhang, Y. Ma, J. Yao, P. de Oliveira, *Carbon* 49 (2011) 1906–1911.
- [19] R. Chetty, S. Kundu, W. Xia, M. Bron, W. Schuhmann, V. Chirila, W. Brandl, T. Reinecke, M. Muhler, *Electrochim. Acta* 54 (2009) 4208–4215.
- [20] J.-P. Tessonnier, D. Rosenthal, F. Girsidis, J. Amadou, D. Beguin, C. Pham-Huu, D. Sheng Su, R. Schlogl, *Chem. Commun.* (2009) 7158–7160.
- [21] D.J. Guo, H.L. Li, *J. Electroanal. Chem.* 573 (2004) 197–202.
- [22] A. Leela Mohana Reddy, S. Ramaprabhu, *J. Phys. Chem. C* 111 (2007) 16138–16146.
- [23] P. Ramesh, M.E. Itkis, J.M. Tang, R.C. Haddon, *J. Phys. Chem. C* 112 (2008) 9089–9094.
- [24] W. Zhu, J.P. Zheng, R. Liang, B. Wang, C. Zhang, G. Au, E.J. Plichta, *J. Electrochem. Soc.* 156 (2009) B1099–B1105.
- [25] X. Zhao, S. Inoue, M. Jinno, T. Suzuki, Y. Ando, *Chem. Phys. Lett.* 373 (2003) 266–271.
- [26] L.M. Sheng, L. Shi, K. An, L.M. Yu, Y. Ando, X.L. Zhao, *Chem. Phys. Lett.* 502 (2011) 101–106.
- [27] R. Sergienko, S. Kim, E. Shibata, T. Nakamura, *J. Nanopart. Res.* 12 (2010) 481–491.
- [28] M.S. Dresselhaus, G. Dresselhaus, R. Saito, A. Jorio, *Phys. Rep.* 409 (2005) 47–99.
- [29] W.F. Chen, J.P. Wang, C.H. Hsu, J.Y. Jhan, H. Teng, P.L. Kuo, *J. Phys. Chem. C* 114 (2010) 6976–6982.
- [30] C.J. Zhong, J. Luo, B. Fang, B. Wanjala, P. Njoki, R. Loukrakpam, J. Yin, *Nanotechnology* 21 (2010) 062001.